

METHODOLOGICAL NOTES

PACS numbers: 42.65.Dr, 42.65.Ky, 42.65.Re, 42.65.Wi

Colors of thin films, antiresonant phenomena in optical systems, and the limiting loss of modes in hollow optical waveguides

A M Zheltikov

DOI: 10.1070/PU2008v051n06ABEH006448

Contents

Abstract. Wave-theory arguments often used to explain colors of thin films are applied to derive simple, physically instructive relations providing a quantitative understanding of transmission spectra of hollow optical waveguides with a complex structure of the cladding. Antiresonant phenomena in complicated optical waveguide systems are shown to weaken the coupling between certain groups of waveguide modes, suggesting ways to substantially reduce optical loss and radically improve the beam quality of radiation transmitted through hollow waveguides. It has been revealed that the presence of a single Fabry – Perot type antiresonant layer in a waveguide cladding considerably lowers the waveguide loss and enhances the suppression of high-order waveguide modes relative to standard, capillary waveguides with a solid cladding. Transmission of optical signals over large distances, however, requires waveguides with a periodically structured antiresonant cladding. The loss in such waveguides exponentially decreases, while the efficiency of high-order mode suppression exponentially increases with the growth in the number of structure periods in the waveguide cladding.

1. Introduction: colors of thin films and guided-wave optics

The excitation efficiency of a resonant system is controlled by a frequency detuning of the driving force from eigenmodes of the system. For a broad class of optical resonators, including various modifications of the Fabry – Perot cavity, resonant excitation of eigenmodes provides a maximum transmission T of an optical signal. In the opposite limiting case, i.e., in the regime of large frequency detuning of a light field from the modes of an optical resonator, the system can display a high reflectivity $R = 1 - T$. This effect is often referred to as an antiresonance.

A well-known experiment that illustrates the change-over of resonant and antiresonant regimes of light action on an optical system involves the observation of the colors of thin films — phenomenon described by Hooke [1], Newton [2], Perot and Fabry [3], Michelson [4], and Fizeau [5] and consistently explained in terms of the wave theory of light by Rayleigh [6]. Light transmitted through a film is a result of multibeam interference of elementary waves (Fig. 1a) that have passed through both interfaces and that have experienced an even number of reflections from the film boundaries. Reflected light, on the other hand, is produced by elementary waves that have passed through the upper film interface twice and that have experienced an odd number of reflections from the film boundaries, as well as by a wave resulting from the reflection of the primary incident wave from the upper boundary of the film. Constructive and destructive interference of reflected and transmitted waves gives rise to colored and dark fringes occurring in reflection and transmission of light, which Rayleigh called the colors of Newton series [7].

Similar to a ray of sunlight, which appears colored upon reflection from a thin film, white light transmitted through the hollow core of an optical waveguide with a complicated structure of cladding often acquires a well-defined color and makes the waveguide cladding glimmer with another color. This simple observation helps us to understand the fundamental properties of a broad class of complex waveguide structures which are receiving an ever-growing application in modern optical technologies.

A M Zheltikov Department of Physics and International Laser Center, M V Lomonosov Moscow State University, Vorob'evy gory, 119992 Moscow, Russian Federation
Tel. (7-495) 939 51 74. Fax (7-495) 939 31 13
E-mail: zheltikov@phys.msu.ru

Received 25 March 2008
Uspekhi Fizicheskikh Nauk **178** (6) 619 – 629 (2008)
DOI: 10.3367/UFNr.0178.200806d.0619
Translated by A M Zheltikov; edited by A Radzig

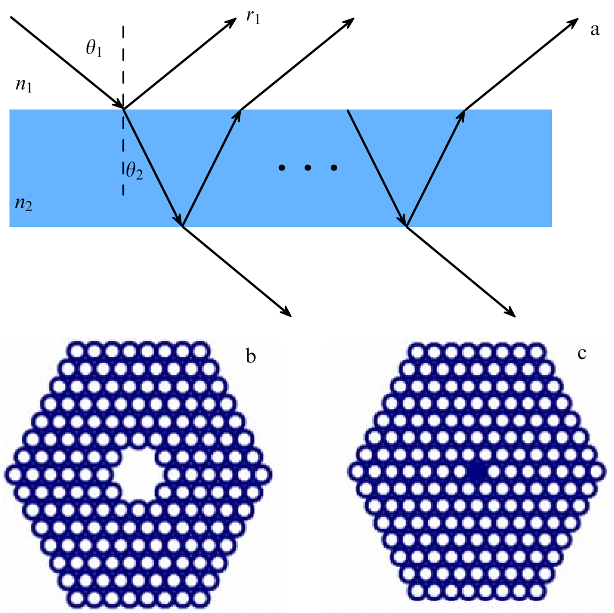

Figure 1. (a) Multiple-beam interference giving rise to colors of a thin film. (b, c) Microstructured waveguides with (b) a hollow core and a photonic-crystal cladding, and (c) a dielectric core.

2. Hollow microstructure waveguides in optical physics

The role of micro- and nanostructured waveguide systems in optical physics has been increasing in its significance through the past years, as such systems have been finding broader and yet broader use in modern optical devices and advanced laser systems [8 – 12]. The development of the technology of photonic-crystal fibers (PCFs) gave rise to a new field in fiber optics, allowing the creation of a novel class of fiber laser systems, frequency converters, generators of broadband radiation, and sources of ultrashort light pulses (see Refs [13, 14] for a review). The key advantages of PCFs for a nonlinear-optical transformation of ultrashort light pulses include the possibilities of engineering the frequency profile of dispersion [15] and the spatial profile of an electromagnetic field [9, 16] in fiber modes through a modification of the fiber structure. Highly efficient PCF-based frequency converters of ultrashort light pulses [17] and sources of radiation with a broad continuous spectrum (supercontinuum) [13, 18 – 21] suggest new solutions to fundamental problems in optical metrology [22 – 25] and ultrafast optics [26] and are actively employed in laser biomedicine [27], as well as in nonlinear spectroscopy [28 – 30] and microscopy [31 – 34]. Along with planar coupled micro- and nanostructured waveguide systems [35, 36], PCFs offer a new attractive platform for optical sensing [37 – 40].

Hollow-core PCFs (Fig. 1b) open new horizons in optical information technologies and high-field physics [9, 41 – 44]. Waveguides of this type are of special interest for the long-distance low-loss transmission of optical signals in the regime of very low optical nonlinearity. Hollow PCFs are employed for the delivery of high-power light pulses in laser systems for biomedical applications [45] and material processing [46]. Simultaneously, work is in progress now on the development of hollow PCFs capable of transmitting mega- and gigawatt optical solitons [47 – 50], as well as hollow waveguide structures for the efficient nonlinear-optical spectral and temporal transformation of high-peak-power ultrashort light pulses [51, 52].

The modes of hollow waveguides are different in their nature from the modes of conventional waveguides, which guide light due to total internal reflection. As the refractive index of the core in hollow waveguides is lower than the refractive index of the cladding, the modes confined in the core of such a waveguide are leaky. These modes are coupled to the cladding modes of the same waveguide. As a result, the imaginary parts of the propagation constants for such modes are nonzero, thus indicating nonzero radiation loss. For standard, capillary type hollow waveguides with a thick cladding, the magnitude of this loss scales as λ^2/a^3 [53] with a core radius a and radiation wavelength λ. As a consequence, only capillary waveguides with a large core diameter are of any interest for practical applications. Such large-core waveguides are, however, essentially multimode.

PCF technology helps to resolve the conflict between the loss and the beam quality of radiation delivered through a hollow waveguide. The generic idea of lowering the loss and improving the beam quality of radiation in hollow waveguides is based on optical antiresonance [13], i.e., weakening the coupling between the modes confined in the core of a waveguide and the cladding modes. As shown in earlier work [55, 56], antiresonant phenomena may have a substantial influence on the mode properties of different types of PCFs and can be employed [57] to reduce the radiation loss of hollow PCFs (see also a review [13]). Regimes of antiresonant waveguiding in solid-core PCFs (Fig. 1c) where the air holes in the cladding are filled with an analyte can be used, as shown by Litchinitser and Poliakov [58], for the creation of novel sensor devices.

The main goal of this work is to demonstrate a unified, physically instructive approach to mode analysis of hollow waveguides with a complex cladding structure. In what follows, we apply wave-theory arguments, which are often used to explain colors of thin films, to provide a quantitative understanding of transmission spectra of hollow optical waveguides with a complicated cladding. We will consider the influence of antiresonance phenomena on the properties of planar (Figs 2a – 2c) and cylindrical (Figs 2d – 2f) hollow waveguides of three types — hollow waveguides with an infinite uniform cladding (Figs 2a, 2d), hollow waveguides with a finite cladding (Figs 2b, 2e), and hollow waveguides with a periodic cladding (Figs 2c, 2f). We will use this approach to show that a single Fabry – Perot type antiresonant layer in a waveguide cladding can considerably lower the waveguide loss and enhance the suppression of high-order waveguide modes relative to standard, capillary waveguides with a uniform cladding. Waveguides with a single antiresonant layer in a cladding offer a convenient platform for novel highly efficient biochemical sensors and frequency converters of high-power ultrashort laser pulses. However, a single antiresonant layer in a waveguide cladding is not sufficient to support low-loss transmission of optical signals over large distances. This challenge can be met through the use of waveguides with a periodically structured antiresonant cladding. The loss in such waveguides exponentially decreases, while the efficiency of high-order mode suppression exponentially increases with the growth in the number of structure periods in the waveguide cladding.

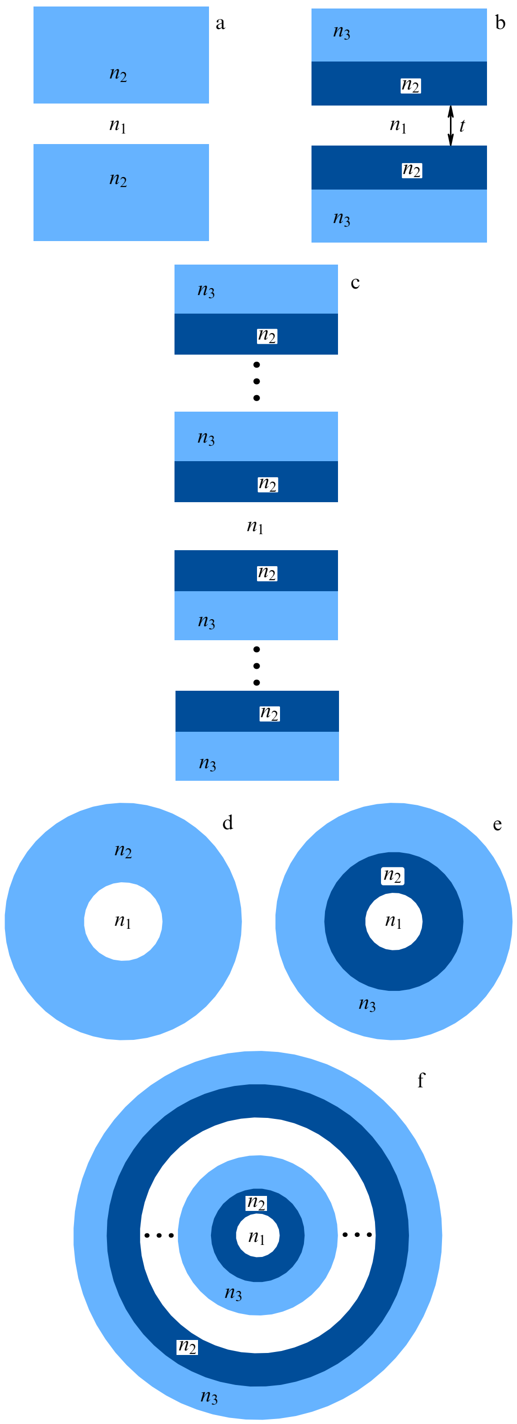

Figure 2. Planar (a – c) and cylindrical (d – f) hollow waveguides consisting of a waveguide layer (core) with a refractive index n_1 and a cladding with a refractive index n_2: (a, d) hollow waveguides with a uniform infinite cladding (material with a refractive index n_2); (b, e) hollow waveguides with a finite cladding, and (c, f) hollow waveguides with a periodic cladding.

3. Ray-optics analysis of hollow waveguides

In this section, we present a simple method for the analysis of radiation loss in hollow waveguides of a general type, based on the ray-optics approximation. Despite its simplicity, this approach lets us derive useful closed-form expressions for the loss coefficient α for the modes of hollow waveguides of

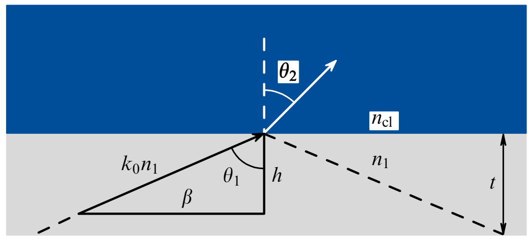

Figure 3. Ray-optics representation of radiation guiding in a hollow waveguide: n_1 and n_{cl} are the refractive indices of the core and the cladding, respectively; θ_1 and θ_2 are the angles that the incident and refracted rays make with the normal to the core – cladding interface; t is the lateral size of the cladding; $\beta = (k_0 n_1^2 - h^2)^{1/2}$ is the propagation constant of the waveguide mode, $k_0 = 2\pi/\lambda$, λ is the radiation wavelength, and h is the eigenvalue of the waveguide mode.

different types, completely coinciding with expressions for α in the case of complex hollow waveguides, obtained by means of a more rigorous, more sophisticated, analysis based on the equations for the transverse field distribution in a waveguide.

Let us consider a generic type of a planar waveguide consisting of a hollow core layer having a refractive index n_1, surrounded by an infinite uniform cladding with a refractive index n_{cl} (Figs 2a, 2d). In a ray-optics picture, a waveguide mode is represented by a zigzag ray trajectory (Fig. 3) where the apex points correspond to a partial reflection of a light ray from the core – cladding interface. As some fraction of radiation energy is transferred through this interface at each point of reflection, the modes of a hollow waveguide are leaky, with the relevant leakage loss α given by [59]

$$\exp(-\alpha L) = r^N , \tag{1}$$

where r is the reflection coefficient of the core – cladding interface, the exponent

$$N = \frac{L}{\tan\theta_1} \tag{2}$$

stands for the number of apex points in the zigzag ray trajectory of length L, and θ_1 is the angle that this ray makes with the normal to the core – cladding interface (Fig. 3).

For a waveguide mode with a propagation constant $\beta = (k_0 n_1^2 - h^2)^{1/2}$, where $k_0 = 2\pi/\lambda$, λ is the radiation wavelength, and h is the mode eigenvalue defined by the relevant characteristic equation (see Fig. 3), we find that

$$\tan\theta_1 = \frac{\beta}{h} . \tag{3}$$

For a planar waveguide with a thickness t of the core layer, this eigenvalue equals

$$h_m = \frac{\pi m}{t} , \tag{4}$$

where m is an integer.

Since the acceptable level of loss in a hollow waveguide is achieved only for the modes represented by zigzag ray trajectories with a grazing incidence of a ray on the core – cladding interface, we assume that $h \ll k_0 n_1$ and reduce Eqn (2) to the following expression

$$N \approx \frac{\lambda m}{2t^2 n_1} L . \tag{5}$$

The reflection coefficient in Eqn (1) is given by the well-known Fresnel formulas which, in the limiting case of $h \ll k_0 n_1$, yield

$$r_{\mathrm{F}} \approx 1 - 4\,\frac{n_1 \cos\theta_1}{n_{\mathrm{cl}} \cos\theta_2} \approx 1 - \frac{2}{(n_{\mathrm{cl}}^2 - n_1^2)^{1/2}}\,\frac{\lambda m}{t}\,, \tag{6}$$

where θ_2 is the angle that the refracted ray makes with the normal to the core – cladding interface (Fig. 3).

Taking logarithms of the left- and right-hand sides of formula (1) and employing an approximation $\ln(1+\xi) \approx \xi$, which is valid for small ξ, we arrive at

$$\alpha_m \approx \frac{1}{(n_{\mathrm{cl}}^2 - n_1^2)^{1/2}}\,\frac{(\lambda m)^2}{t^3 n_1}\,. \tag{7}$$

Expression (7), which was derived using simple ray-optics arguments, coincides with the result of more rigorous analysis based on the characteristic equation for complex propagation constants of modes in a planar hollow waveguide [53]. The leakage loss of a cylindrical hollow waveguide with an inner diameter t (Fig. 2d) can be found by multiplying the loss coefficient defined by Eqn (7) by a quantity $(2u_l/\pi m)^2$, where u_l is the upper limit for the mode eigenvalue for the lth mode of a cylindrical waveguide [for the fundamental mode, $l = 0$ and $J_0(u_0) = 0$)].

As can be seen from expression (7), the leakage loss of a mode in a hollow waveguide scales as the square of the radiation wavelength and is inversely proportional to the third power of the lateral size of the waveguide core layer. For high-order modes, as may also be seen from Eqn (7), the leakage loss grows with the square of the mode index m. This circumstance allows one to filter the fundamental waveguide mode and suppress higher order modes by choosing the waveguide length L in such a way that $\alpha_2^{-1} < L < \alpha_1^{-1}$. For gas-filled hollow waveguides with a silica cladding ($n_1 \approx 1$, $n_{\mathrm{cl}} \approx 1.45$), formula (7) yields the following simple expression for the attenuation length in the case of the fundamental waveguide mode: $l_1 = \alpha_1^{-1} \approx t^3/\lambda^2$. For hollow waveguides with a large core ($t = 100\lambda = 100$ μm), we thus find $l_1 \approx 1$ m. Such waveguides are successfully employed for the compression of high-power ultrashort laser pulses [60, 61]. With $t = 10\lambda = 10$ μm, we, however, arrive at $l_1 \approx 1$ mm. These estimates show that hollow waveguides with a uniform infinite silica cladding are not suitable for the long-distance transmission of optical signals. We will show in the following sections that an antiresonant structure of a cladding can substantially lower the leakage loss and considerably improve the beam quality of radiation transmitted through a hollow waveguide.

4. Antiresonant phenomena in a hollow waveguide with a finite cladding

Consider now a waveguide structure consisting of a hollow core with a refractive index n_1 and a lateral size t, and a cladding with a finite layer thickness d and a refractive index n_2 (Figs 2b, 2e). We assume for simplicity that the refractive index n_3 of a medium outside the above-mentioned cladding layer is close to the refractive index n_1 of the core. Physically, the difference between a hollow waveguide with a finite cladding (Figs 2b, 2e) and a hollow waveguide with an infinite cladding (Figs 2a, 2d) is related to the reflection of light from the outer boundary of the cladding. As shown below in this section, the interference of the fields reflected from the cladding boundaries can substantially lower the leakage loss of a hollow waveguide. We analyze a hollow waveguide with a finite cladding using Eqn (1), where the well-known formula of a Fabry – Perot etalon is employed to describe reflection from a finite cladding layer:

$$r \approx r_{\mathrm{FP}} = \frac{F \sin^2(\delta/2)}{1 + F \sin^2(\delta/2)}\,. \tag{8}$$

Here, the following notation was introduced:

$$\delta = \frac{4\pi}{\lambda}\,d n_2 \left\{1 - \left(\frac{n_1}{n_2}\right)^2 \left[1 - \left(\frac{h}{\beta}\right)^2\right]\right\}^{1/2}, \tag{9}$$

$$F = \frac{4 r_{\mathrm{F}}}{(1 - r_{\mathrm{F}})^2}\,, \tag{10}$$

and r_{F} is the reflection coefficient calculated by the Fresnel formulas (6).

In the regime of grazing incidence ($\theta_1 \ll 1$, $h \ll \beta$), expressions (9) and (10) may be reduced to

$$\delta \approx \frac{4\pi}{\lambda}\,d\,(n_2^2 - n_1^2)^{1/2}\,, \tag{11}$$

$$F \approx \frac{t^2}{\lambda^2}\,(n_2^2 - n_1^2)\,. \tag{12}$$

The solid line in Fig. 4 displays the transmission spectrum $T(\lambda) = \exp(-\alpha L)$ calculated using Eqns (1), (5), (8) – (10) for the fundamental mode ($m = 1$) of the considered planar hollow waveguide with $n_1 = 1$, $t = 10$ μm, $d = 0.5$ μm, and $L = 2$ cm. The dispersion of the cladding was included in these calculations by using the Sellmeier equation for fused silica.

The equality

$$\lambda_l = \frac{2d}{l}\,(n_2^2 - n_1^2)^{1/2}\,, \tag{13}$$

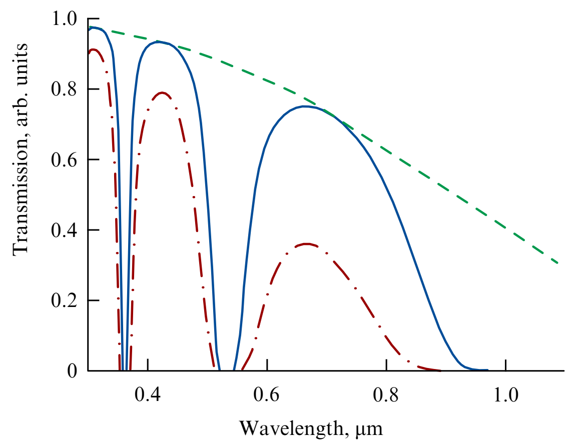

Figure 4. Transmission spectra of a planar (solid and dashed lines) and a cylindrical (dash-and-dot line) hollow waveguide with a single antiresonant layer in the cladding. For a planar waveguide, calculations were performed by using Eqns (1), (5), (8) – (10) (solid line) and Eqn (15) (dashed line). The dispersion of the cladding was included by using the Sellmeier equation for fused silica. The refractive index of the core is $n_1 = 1$. The lateral size of the core equals $t = 10$ μm. The thickness of the antiresonant layer amounts to $d = 0.5$ μm. The length of the waveguide is $L = 2$ cm.

where l is an integer, specifies the conditions of a resonant excitation of Fabry–Perot cavity modes of the waveguide cladding. In this regime, the modes confined in the waveguide core are strongly coupled to cladding modes and rapidly leak to the cladding, giving rise to well-pronounced minima in the transmission spectrum of the waveguide (Fig. 4).

By contrast, around the wavelengths

$$\lambda_j = \frac{4d}{2j+1}\,(n_2^2 - n_1^2)^{1/2}\,, \tag{14}$$

where j is an integer, the coupling between the core and cladding modes is reduced to a minimum. When the condition specified by formula (14) is satisfied, Fabry–Perot cavity cladding modes are antiresonant to the core modes [55, 56], providing a maximum transmission of the waveguide modes (Fig. 4).

Substituting expression (8) into formula (1) and using Eqns (6) and (10), we find for the antiresonant waveguiding regime, defined by condition (14), that

$$\alpha_m^{\mathrm{ar}} \approx \frac{1}{2(n_2^2 - n_1^2)}\,\frac{(\lambda m)^3}{t^4 n_1}\,. \tag{15}$$

Formula (15) coincides with the expression for the leakage loss of a planar waveguide with a finite cladding, derived by solving the relevant characteristic equation [62, 63]. As can be seen from formula (15), the leakage loss of an antiresonant finite-cladding hollow waveguide (the dashed line in Fig. 4) scales as the third power of the radiation wavelength and is inversely proportional to the fourth power of the lateral size of the waveguide core. For high-order modes, as may also be seen from formula (15), the leakage loss grows as the third power of the mode index m. An antiresonant waveguide cladding thus substantially (by a factor of λ/m) reduces the loss of waveguide modes as opposed to a hollow waveguide with an infinitely thick uniform cladding. Due to the scaling $\alpha_m^{\mathrm{ar}} \propto m^3$, an antiresonant waveguide cladding also enhances the suppression of high-order waveguide modes when compared to a standard hollow waveguide with an infinite cladding [cf. formulas (7) and (15)].

The leakage loss of a cylindrical hollow waveguide with an inner diameter t (Fig. 2e) can be found by multiplying the loss coefficient of a planar finite-cladding hollow waveguide by a quantity $(2u_l/\pi m)^3$, where u_l is the upper limit for the mode eigenvalue for the lth mode of a cylindrical waveguide. The transmission spectrum of a cylindrical waveguide with an inner diameter $t = 10$ μm and an outer diameter of 11 μm, and with $n_1 = 1$ and $L = 2$ cm is shown by the dashed–dotted line in Fig. 4.

Although a hollow waveguide with an antiresonant cladding can substantially reduce the leakage loss as compared to a hollow waveguide with a uniform infinite cladding, the level of loss in an antiresonant-cladding waveguide remains too high for the long-distance transmission of optical signals, as the lateral size of the waveguide core becomes as small as a few radiation wavelengths. Indeed, setting $n_1 \approx 1$, $n_2 \approx 1.45$, and $t = 10\lambda = 10$ μm for a gas-filled hollow waveguide with a silica cladding, we find from formula (15) that $l_1^{\mathrm{ar}} = (\alpha_1^{\mathrm{ar}})^{-1} \approx 2$ cm. With $t = 30\lambda = 10$ μm, the l_1^{ar} parameter reaches 1.6 m, which is still not enough for the long-distance transmission of optical signals. In Section 5, we will demonstrate that the problem of long-distance optical transmission can be solved by using hollow waveguides with a periodically structured cladding.

5. A hollow waveguide with a periodic cladding

We now examine a hollow waveguide where the cladding consists of periodically alternating planar (Fig. 2c) or cylindrical (Fig. 2f) layers having refractive indices n_1 and n_2 and thicknesses a and b. A cladding with such a structure qualifies as a one-dimensional photonic crystal. Within finite frequency ranges, the destructive interference of light waves transmitted through the interfaces between the planar or cylindrical layers forming the photonic-crystal cladding of the waveguide cancels the radiation field inside the structure. In these frequency ranges, called photonic band gaps (PBGs), the photonic-crystal structure exhibits a high reflectivity. This property of periodic structures helps us to reduce the leakage loss of modes in hollow waveguides with a coaxial Bragg cladding [64, 65] or a two-dimensionally periodic cladding [41–44].

Planar and coaxial Bragg waveguides can be conveniently analyzed by employing well-developed numerical methods [65, 66], as well as approximate semianalytical approaches [67–69] based on the transfer-matrix technique. Here, we will follow the general idea of this work and examine the properties of modes in Bragg-cladding hollow waveguides using the ray-optics approach described in the previous sections. Below, we will apply the ray-optics analysis to find the leakage loss of Bragg-cladding hollow waveguides starting from the reflection coefficients of a periodic cladding, calculated by utilizing the transfer-matrix technique. For the planar photonic-crystal structure shown in Fig. 2c, such a transfer-matrix analysis yields [59]

$$r = r_{\mathrm{PBG}} = \frac{G}{G + (\sin K\Lambda/\sin MK\Lambda)^2}\,, \tag{16}$$

where $\Lambda = a + b$ is the period of the structure in the cladding, and M is the number of periods (unit cells) of the cladding,

$$G = \frac{r_1}{1 - r_1}\,, \tag{17}$$

$$r_1 = \left|\frac{C}{A}\right|^2 \tag{18}$$

is the coefficient of reflection from a unit cell of the photonic-crystal structure,

$$K = \frac{1}{\Lambda}\arccos\frac{A + D}{2} \tag{19}$$

is the Bloch wave number defining the radiation field inside the periodic structure,

$$A = \exp(\mathrm{i}k_1 a)\left[\cos k_2 b + \frac{\mathrm{i}}{2}\left(\frac{k_2}{k_1} + \frac{k_1}{k_2}\right)\sin k_2 b\right], \tag{20}$$

$$C = \frac{\mathrm{i}}{2}\exp(\mathrm{i}k_1 a)\left(\frac{k_1}{k_2} - \frac{k_2}{k_1}\right)\sin k_2 b\,, \tag{21}$$

$$D = \exp(-\mathrm{i}k_1 a)\left[\cos k_2 b - \frac{\mathrm{i}}{2}\left(\frac{k_2}{k_1} + \frac{k_1}{k_2}\right)\sin k_2 b\right] \tag{22}$$

are the elements of the transfer matrix for the layered structure of the cladding, and

$$k_i = 2\pi\lambda^{-1} n_i \cos\theta_i\,, \quad i = 1, 2\,.$$

It is evident from expressions (19)–(22) that the Bloch wave numbers K become complex (Fig. 5) within the PBGs

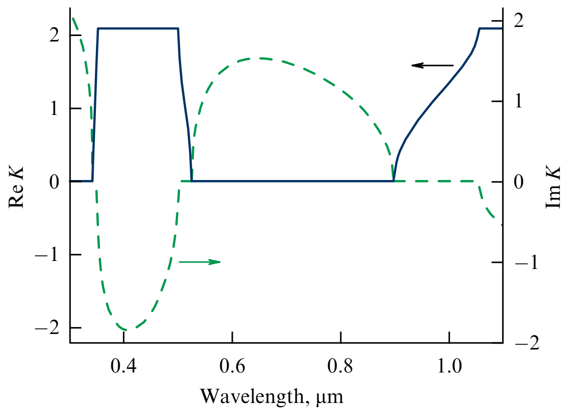

Figure 5. Spectra of the real (solid line) and imaginary (dashed line) parts of the Bloch wave number K for a periodic waveguide cladding with $a = 1$ μm, $b = 0.5$ μm, $n_1 = 1$, and $n_2 = 1.45$.

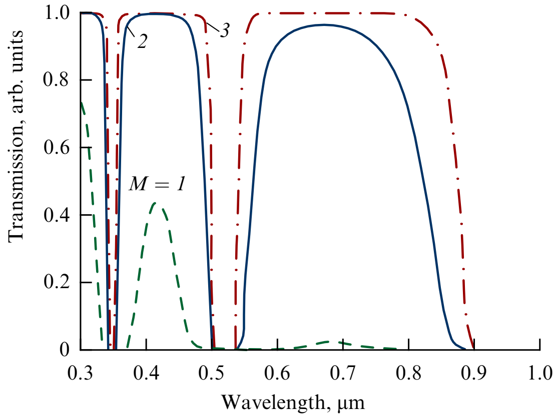

Figure 6. Transmission spectrum of a hollow waveguide with a periodic cladding with $t = 10$ μm, $a = 1$ μm, $b = 0.5$ μm, $n_1 = 1$, $n_2 = 1.45$, and $M = 1$ (dashed line), *2* (solid line), and *3* (dash-and-dot line).

defined by the condition $K\Lambda = \pi l$, where l is an integer:

$$K = \frac{\pi l}{\Lambda} + \mathrm{i}K' , \tag{23}$$

where K' is the imaginary part of the Bloch wave number [59].

Within the PBG, in accordance with expression (23), the radiation field inside the periodic waveguide cladding exponentially decays with the distance from the core – cladding interface. In this frequency range, no real Bloch wave number is allowed for a light field inside the cladding structure (see Fig. 5), which thus becomes antiresonant to waveguide modes confined in the hollow core of the waveguide.

When $1 - r_1 \ll 1$, formula (16) can be conveniently rewritten as

$$r_{\mathrm{PBG}} = 1 - \frac{1 - r_1}{r_1} \left(\frac{\sin K\Lambda}{\sin MK\Lambda} \right)^2 . \tag{24}$$

Expression (24) provides useful insights into the role of a periodic structure, which furnishes a high reflectivity of the waveguide cladding.

For $M = 1$, expression (16) is reduced to $r_{\mathrm{PBG}} = r_1 \approx r_{\mathrm{FP}}$. The transmission spectrum of the fundamental waveguide mode then tends to the transmission spectrum of a hollow waveguide with a single antiresonant layer in the cladding (the dashed line in Fig. 6). The solid and dashed – dotted lines in Fig. 6 depict transmission spectra for the fundamental ($m = 1$) mode of a periodic-cladding hollow waveguide with $t = 10$ μm, $a = 1$ μm, $b = 0.5$ μm, $n_1 = 1$, and $n_2 = 1.45$ calculated for three values of M using Eqns (1), (5), and (16) – (22). As can be seen from the results presented in this figure, a periodic cladding can considerably lower the leakage loss of a waveguide mode as compared to a hollow waveguide with a single antiresonant layer in the cladding.

At the PBG edges, where $K\Lambda = \pi l$, with l being an integer, the reflection coefficient of a periodic cladding is given by

$$r_{\mathrm{PBG}} = \frac{r_1}{r_1 + (1 - r_1)/M^2} . \tag{25}$$

As $1 - r_1 \ll 1$, we arrive at

$$r_{\mathrm{PBG}} \approx 1 - \frac{1}{M^2} \, \frac{1 - r_1}{r_1} . \tag{26}$$

Using expression (18), we can then represent the leakage loss of the waveguide modes as

$$\alpha_m^{\mathrm{PBG}} \approx \frac{1}{2(n_2^2 - n_1^2)} \, \frac{(\lambda m)^3}{t^4 n_1} \, \frac{1}{M^2} . \tag{27}$$

Within a PBG, formula (16) is reduced to

$$r = r_{\mathrm{PBG}} = \frac{G}{G + (\sinh K\Lambda / \sinh MK\Lambda)^2} . \tag{28}$$

When $1 - r_1 \ll 1$ and $M \gg 1$, Eqn (28) yields

$$r_{\mathrm{PBG}} \approx 1 - \frac{1 - r_1}{r_1} \exp\left[-2(M - 1)\, K'\Lambda \right] . \tag{29}$$

Substituting expression (29) into formula (1) and using expression (18), we finally arrive at

$$\alpha_m^{\mathrm{PBG}} \approx \frac{1}{2(n_2^2 - n_1^2)} \, \frac{(\lambda m)^3}{t^4 n_1} \exp\left[-2(M - 1)\, K'\Lambda \right] . \tag{30}$$

As can be seen from formulas (27) and (30), an increase in the number of layers in the periodic structure of the cladding leads to a rapid lowering of the waveguide loss inside the PBG (see also Fig. 6). At the center of the PBG, where the coupling between the core and cladding modes involves tunneling through an extended antiresonant cladding structure, the waveguide loss decreases exponentially with increasing the number of layers in the cladding.

The level of leakage loss provided by silica hollow waveguide structures with a periodic cladding appears to be low enough to allow a long-distance transmission of optical signals. In particular, silica waveguide structures with $t = 10\lambda$ and $M \geqslant 4$ meet the standard requirements for long-distance data transmission in the fundamental waveguide mode ($m = 1$): $l_1^{\mathrm{PBG}} = (\alpha_1^{\mathrm{PBG}})^{-1}$.

6. Optical components and devices based on hollow waveguides with an antiresonant cladding

We now employ the results of the analysis of the properties of hollow microstructure waveguides, performed in the previous sections, to understand possible applications of such waveguide systems. Typical images of hollow waveguides with a microstructured cladding fabricated by means of PCF technologies [42, 66, 70, 71] are presented in Fig. 7. The inner part of the cladding that is adjacent to the waveguide core and that has the shape of a ring 1 – 2 μm thick plays the key role determining the properties of waveguide modes for the considered class of waveguides. The solid line in Fig. 8 shows a typical transmission spectrum measured for such a waveguide structure, featuring a sequence of well-resolved maxima and minima. The wavelengths and the bandwidths of these features are adequately described in terms of the model of a ring-cladding hollow waveguide (the dashed line in Fig. 8). The sequence of maxima and minima in the transmission spectrum of the waveguide considered corresponds to a Newton series of thin-film colors, with the ring-shaped inner part of the cladding (Fig. 7) playing the role of such a film in the waveguide structure under consideration.

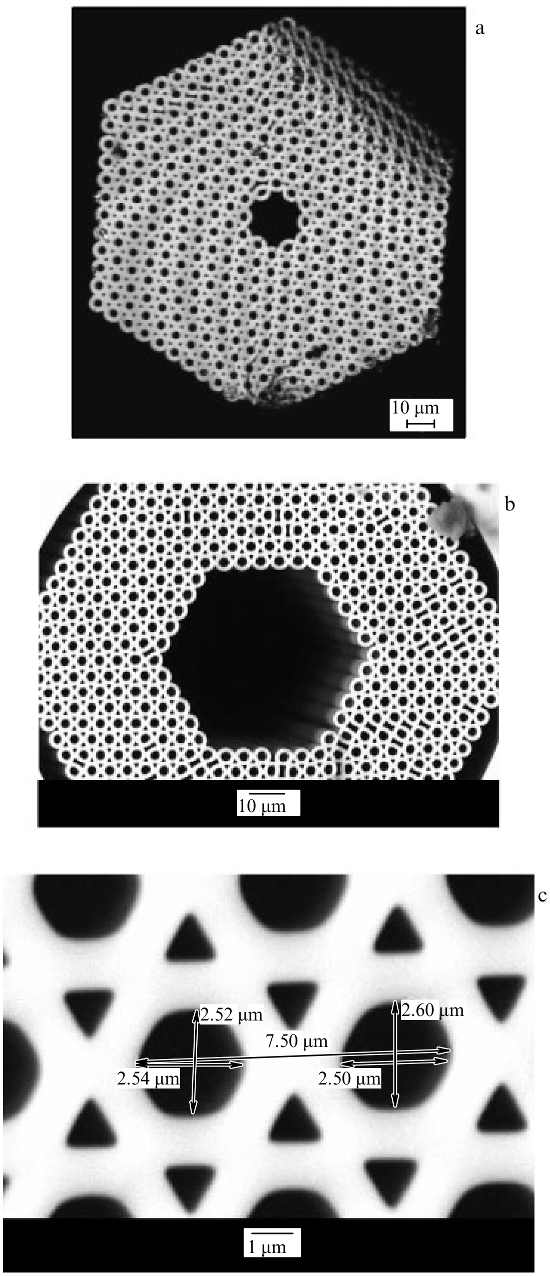

Figure 7. Cross-section images of hollow waveguides with a microstructured cladding: (a, b) the general view, and (c) close-up view of the cladding.

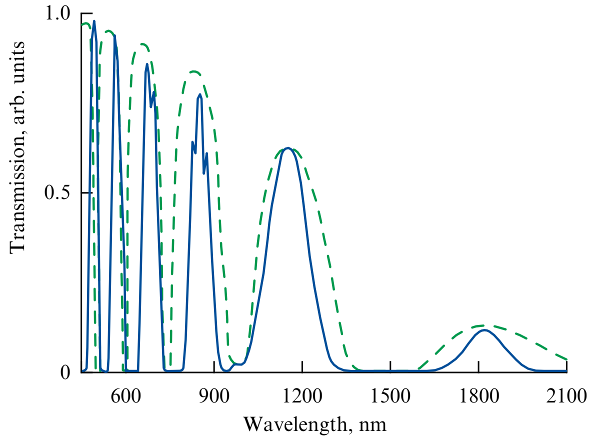

Figure 8. Transmission spectrum of a hollow waveguide with the cross-section structure shown in Fig. 7a: the solid line fits experimental data, and the dashed line fits calculated results obtained using formulas (1), (5), and (8) – (10) for $t = 20$ μm and $d = 1.4$ μm.

The waveguide structure presented in the inset to Fig. 9 [72, 73] implements the idea of an antiresonant suppression of coupling between the mode localized in the hollow core and the extended cladding of the waveguide structure having the form of a two-dimensional periodic structure. The transmission spectrum of this waveguide is displayed in Fig. 9. The optical loss for hollow waveguides of this type is much lower than the loss of optical waveguides with a single antiresonant layer in the cladding. With advanced PCF technologies at hand [57], the level of leakage loss for this type of structures can be reduced to 1 dB km^{-1}.

Hollow waveguides with a photonic-crystal cladding have been shown to support stable isolated guided modes of high-power ultrashort light pulses [9, 13, 44] and to perform efficient nonlinear-optical transformations of such light fields [47, 74 – 78]. Waveguides of this type have also been used for the creation of high-power frequency-tunable optical solitons [47, 48, 79]. Hollow PCFs with a low optical nonlinearity and a tailored dispersion profile offer much promise as dispersion-compensating components and pulse

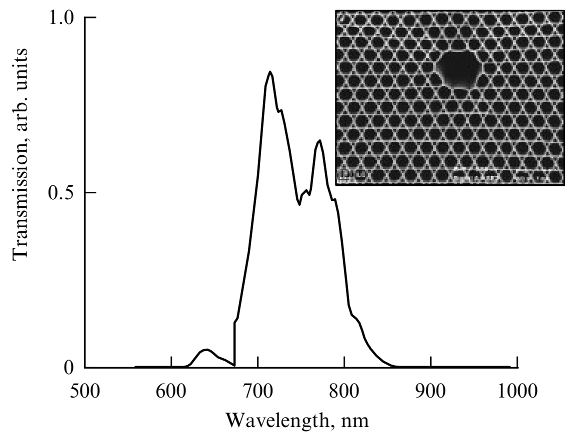

Figure 9. Transmission spectrum of a hollow waveguide with the cross-section structure shown in the inset to the figure.

compressors for high-power fiber laser systems [80–82]. Fiber-optic waveguides of this class can also transmit high-power nano- and picosecond pulses in optical systems designed for biomedical [45] and technological applications [46] and suggest attractive solutions for the creation of a new type of fiber-optic endoscope.

Due to their interference origin, the maxima and minima in transmission spectra of ring-cladding hollow waveguides are highly sensitive to small changes in the thickness of the cladding ring surrounding the core, as well as to small variations in the refractive index of the material filling the hollow core and the holes in the waveguide cladding. This suggests an attractive approach to sensing biochemical reactions in a solution filling the air holes of a waveguide, e.g., the air holes in a hollow-core PCF. Below, we will examine two types of sensing devices based on ring-cladding hollow waveguides. Sensors of the first type are intended to detect thin layers of biomolecules immobilized on the waveguide walls. Sensors of the second type detect small changes in the refractive index of an analyte filling the air holes in the waveguide structure.

Operation of the sensor of the first type is illustrated in Fig. 10. Formation of a biomolecular layer on the surface of a ring cladding of a hollow waveguide as a result of biochemical processes in an analyte solution filling the air holes in the waveguide (see the inset to Fig. 10) shifts minima in the transmission spectrum of the waveguide (Fig. 10). Creation of DNA sensors based on this principle faces difficulty related to the fact that DNA molecules, which contain negatively charged phosphate groups, cannot be directly immobilized on the surface of fused silica because the surface also carries a negative charge. This problem can often be solved by utilizing poly-L-lysin [40], which contains positively charged amino groups, assisting in the formation of a molecular monolayer on a negatively charged silica surface. Such a monolayer helps to immobilize DNA molecules on a silica waveguide wall (the inset to Fig. 10), giving rise to a molecular layer with a thickness of about 10 nm and a refractive index (1.45–1.48)

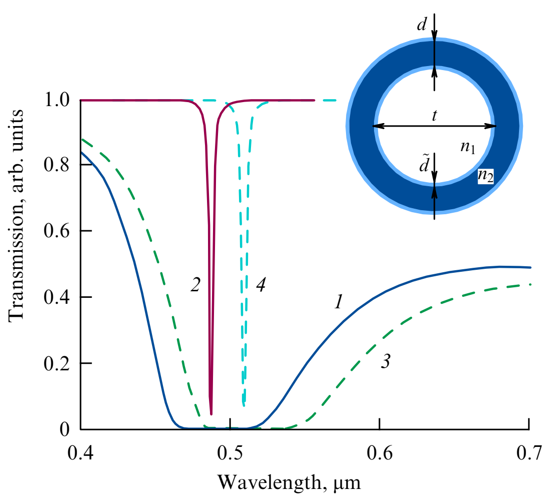

Figure 10. Transmission spectra of a ring-cladding hollow waveguide (shown in the inset) filled with an analyte characterized by a refractive index $n_1 = 1.33$ without (*1*, *2*) and with (*3*, *4*) a 10-nm-thick layer of biomolecules on both sides of the cladding. The ring-cladding thickness is $d = 400$ nm, the refractive index of the cladding equals $n_2 = 1.46$. The lateral size of the core is $t = 15$ μm (*1*, *3*) and 100 μm (*2*, *4*).

close [40] to the silica refractive index. Formation of such a layer in a solution filling the air holes in the waveguide structure can be detected from the spectral shift of transmission bands of the ring-cladding hollow waveguide (see Fig. 10).

The factor F, defined by formula (10), is the key parameter controlling the sensitivity of the considered type of a waveguide sensor, as it determines the visibility of interference fringes produced by multiple reflections from the Fabry–Perot-cavity cladding of the waveguide. For the modes of a hollow waveguide corresponding to a grazing incidence of light on the core–cladding interface ($\theta_1 \ll 1$, $h \ll \beta$), the factor F is given by formula (12). As can be seen from this formula, the transmission spectrum of the ring-cladding hollow waveguide features narrow dips for large t/λ ratios, corresponding to a resonant excitation of Fabry–Perot cavity modes in the ring cladding of the waveguide. In this regime, ultrathin molecular layers formed on the cladding surface as a result of biochemical processes can be detected.

We now assume that the immobilization of DNA on a poly-L-lysin monolayer formed on both surfaces of the ring cladding of the waveguide results in the formation of a layer with a thickness $\tilde{d}$ (see the inset to Fig. 10) and a refractive index close to the refractive index of the cladding. Effectively, this corresponds to an increase in the cladding thickness by $2\tilde{d}$. Around a resonance (13) with Fabry–Perot-type modes of ring cladding, providing a minimum in the transmission capacity of the waveguide, we find [84] that $\delta/2 = \pi l + \xi/2$, where $\xi \approx 8\pi\tilde{d}\lambda^{-1}(n_2^2 - n_1^2)^{1/2}$ is a small parameter, so that $\sin^2(\delta/2) \approx \xi^2/4$. The minimal detectable shift of the relevant dip in the transmission spectrum of a waveguide can be defined as the spectral width $\delta\lambda$ of the transmission minimum, which can be estimated from the relationship $F\sin^2(\delta/2) \approx F\xi^2/4 = 1$.

Using this expression, we can derive a simple approximate formula for the minimal detectable thickness of a biomolecular layer on the cladding surface: $\tilde{d}_m \approx [4\pi t(n_2^2 - n_1^2)]^{-1}\lambda^2$. For a hollow waveguide filled with an analyte with a refractive index $n_1 \approx 1.33$ and having a ring cladding with a refractive index $n_2 \approx 1.46$ (see the inset to Fig. 10), the minimal detectable thickness of a layer of immobilized biomolecules is then estimated as $\tilde{d}_m \approx 0.13\lambda^2/t$. With $\lambda = 0.5$ μm and $t = 100$ μm, one finds that $\tilde{d}_m \approx 0.3$ nm.

For a waveguide with $n_1 \approx 1.33$ and $n_2 \approx 1.46$, having an unperturbed cladding thickness $d = 400$ nm, the minimum of transmission corresponding to $l = 1$ is observed at the wavelength $\lambda_1 \approx 480$ nm (curves *1* and *3* in Fig. 10). Formation of a layer of immobilized DNA molecules with a thickness of $\tilde{d} \approx 10$ nm on both surfaces of the waveguide cladding shifts the transmission minimum by $\Delta\lambda = 4\tilde{d}(n_2^2 - n_1^2)^{1/2} \approx 24$ nm (Fig. 10).

Waveguide sensors of the second type are intended for the detection of small changes in the refractive index of an analyte filling the air holes in the waveguide structure. A small change δn in the refractive index of the analyte shifts the minima in the transmission spectrum of a ring-cladding waveguide (Fig. 11). This shift $\Delta\lambda$ can be found by differentiating expression (13) in n_1. This procedure yields $\delta\lambda = 2dm^{-1}n_1(n_2^2 - n_1^2)^{1/2}\delta n$. For a small change in the refractive index of an analyte around a resonance (13) with Fabry–Perot modes of the ring cladding, providing a minimum in the transmission capacity of a waveguide, we derive $\delta/2 = \pi l + \zeta/2$, where $\zeta \approx -4\pi d\lambda^{-1}n_1\delta n(n_2^2 - n_1^2)^{-1/2}$ is a small parameter, so that $\sin^2(\delta/2) \approx \zeta^2/4$. The minimum

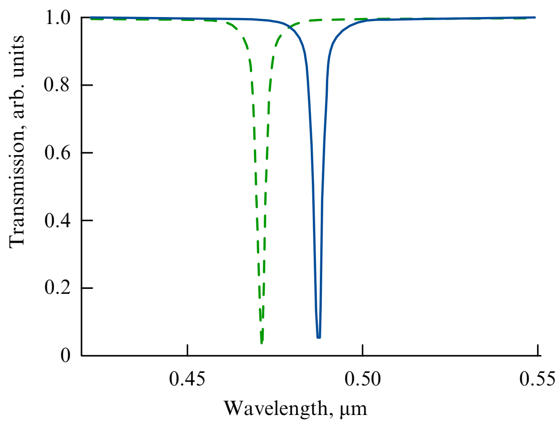

Figure 11. Transmission spectra of a ring-cladding hollow waveguide filled with an analyte with a refractive index $n_1 = 1.33$ (solid line) and $n_1 = 1.34$ (dashed line). The thickness of the ring cladding of the waveguide is $d = 400$ nm, the refractive index of the cladding equals $n_2 = 1.46$. The lateral size of the core is $t = 100$ μm.

change in the refractive index that can still be detected by such a sensor is controlled by the parameter F and may be found from the equation $F\sin^2(\delta/2) \approx F\zeta^2/4 = 1$. Solving this equation and using formula (12), we arrive at $|\delta n| \approx \lambda^2(2\pi n_1 dt)^{-1}$. With $n_1 = 1.33$, $\lambda = 0.5$ μm, $d = 0.4$ μm, and $t = 100$ μm, we find that $|\delta n| \approx 7 \times 10^{-4}$. Importantly, in contrast to many types of integrated antiresonant reflecting optical waveguide sensors [36], the proposed sensor design does not require an external interferometer, because a Fabry – Perot interferometer is, in fact, built-in to the waveguide cladding of the sensor device considered.

Figure 12 presents a structure that integrates ring-cladding hollow waveguides with a hollow-core diameter increasing from the center of the structure to its periphery [85]. The central part of the structure includes an array of ring-cladding hollow waveguides with an outer diameter of about 10 μm. This part of the structure is surrounded with six arrays of ring-cladding waveguides with an outer diameter of about 20 μm. The diameter of hollow waveguides reaches 200 μm in outer sections of this structure. Such a system of hollow waveguides enables the parallel detection of various biochemical processes in a solution on a platform of a single chip.

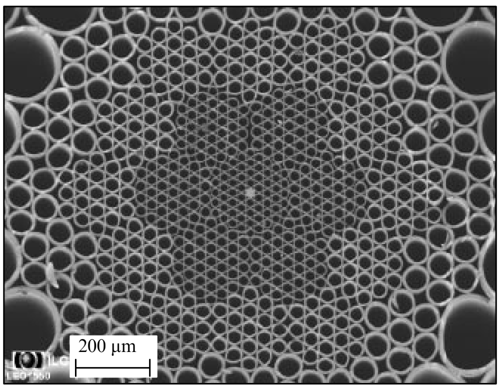

Figure 12. Cross-section image of structure-integrated arrays of hollow waveguides enabling a parallel detection of different biochemical processes in a solution on a platform of a single chip.

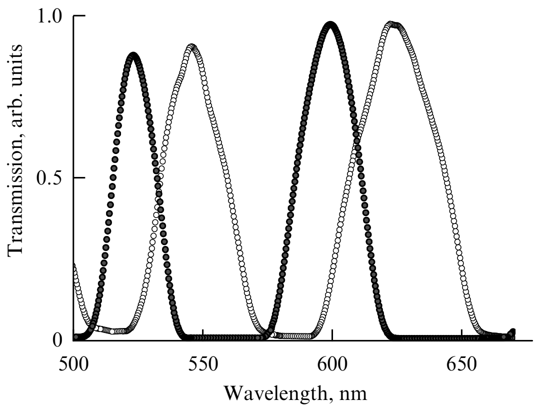

Figure 13. Transmission spectra of hollow microstructure waveguides with different thicknesses of the ring-shaped structure of the inner part of the cladding adjacent to the waveguide core.

Measurement data presented in Fig. 13 illustrate a shift in the transmission band of a hollow waveguide with the cross-section structure shown in Fig. 7a, caused by a change in the thickness of the inner ring-shaped part of its cladding. These data suggest a high sensitivity of transmission spectra of hollow microstructure waveguides to variations in the thickness of the inner ring-shaped part of the cladding bounding the hollow core of the waveguide.

7. Conclusion

In this paper, we applied the wave-theory arguments explaining colors of thin films to derive simple, physically instructive relations providing a quantitative understanding of transmission spectra of hollow optical waveguides with a complex structure of the cladding. Our analysis shows that an antiresonant structure of the waveguide cladding can substantially reduce optical loss and radically enhance the suppression of high-order modes in complex systems of hollow waveguides. It has been shown that waveguides with a single Fabry – Perot type antiresonant layer in a cladding allow novel highly efficient biochemical sensors and frequency converters of high-power ultrashort laser pulses to be implemented. Transmission of optical signals over large distances, however, requires waveguides with a periodically structured antiresonant cladding. Optical coupling between the core and cladding modes in such waveguide structures involves a tunneling of the light field through an extended antiresonant cladding. As a consequence, the loss in such waveguides exponentially decreases, while the efficiency of high-order mode suppression exponentially increases with the growth in the number of structure periods in the waveguide cladding.

Acknowledgments. I am pleased to gratefully acknowledge fruitful collaboration and illuminating discussions with A B Fedotov and D A Sidorov-Biryukov (Department of Physics, M V Lomonosov Moscow State University), A A Ivanov and M V Alfimov (Center of Photochemistry, Russian Academy of Sciences), P St J Russell (University of Erlangen — Nuremberg), A Baltuška (Technological University of Vienna), F Krausz (Max Planck Institute for Quantum Optics, Garching), R Miles and M Shneider (Princeton University), D von der Linde and A P Tarasevitch (University of Essen — Duisburg), J C Knight (University of

Bath), D Reid (Heriott – Watt University, Edinburgh), V S Shevandin and K V Dukel'skii (S I Vavilov State Optical Institute, St.-Petersburg), and V I Beloglazov, N B Skibina, and A V Shcherbakov (Institute of Technology and Equipment for Glass Structures, Saratov).

This study was supported in part by the Russian Foundation for Basic Research (project Nos 06-02-16880, 07-02-12175, 06-02-39011, 07-02-91215, and 05-02-90566-NNS) and the Russian Federal Research and Technology Program (contract No. 02.513.11.3040).

References

1. Hooke R *Micrographia: or, Some Physiological Descriptions of Minute Bodies Made by Magnifying Glasses* (London: J. Martyn and J. Allestry, 1665)
2. Newton I *Optics: or, A Treatise of the Reflections, Refractions, Inflections and Colours of Light* (London: Smith and Walford, 1704)
3. Perot A, Fabry C *Ann. Chim. Phys.* **16** 289 (1899)
4. Michelson A A *Philos. Mag.* **13** 236 (1882)
5. Fizeau A H *C.R. Acad. Sci.* **66** 934 (1868)
6. Rayleigh J W *Philos. Mag.* **28** 200 (1889)
7. Rayleigh J W, in *Encyclopedia Britannica* 9th ed. (New York, 1888)
8. Knight J C et al. *Science* **282** 1476 (1998)
9. Russell P *Science* **299** 358 (2003)
10. Knight J C *Nature* **424** 847 (2003)
11. Zheltikov A M *Usp. Fiz. Nauk* **170** 1203 (2000) [*Phys. Usp.* **43** 1125 (2000)]
12. Zheltikov A M *Optika Mikrostrukturirovannykh Volokon* (Optics of Microstructured Fibers) (Moscow: Nauka, 2004)
13. Russell P St J *J. Lightwave Technol.* **24** 4729 (2006)
14. Zheltikov A M *Usp. Fiz. Nauk* **177** 737 (2007) [*Phys. Usp.* **50** 705 (2007)]
15. Reeves W H et al. *Nature* **424** 511 (2003)
16. Fedotov A B, Zheltikov A M, Tarasevitch A P, von der Linde D *Appl. Phys. B* **73** 181 (2001)
17. Zheltikov A M *Usp. Fiz. Nauk* **174** 73 (2004) [*Phys. Usp.* **47** 69 (2004)]
18. Ranka J K, Windeler R S, Stentz A J *Opt. Lett.* **25** 796 (2000)
19. Zheltikov A M (Ed.) "Supercontinuum Generation" *Appl. Phys. B* **77** (Special Iss., 2/3) (2003)
20. Zheltikov A M *Usp. Fiz. Nauk* **176** 623 (2006) [*Phys. Usp.* **49** 605 (2006)]
21. Dudley J M, Genty G, Coen S *Rev. Mod. Phys.* **78** 1135 (2006)
22. Jones D J et al. *Science* **288** 635 (2000)
23. Holzwarth R et al. *Phys. Rev. Lett.* **85** 2264 (2000)
24. Diddams S A et al. *Phys. Rev. Lett.* **84** 5102 (2000)
25. Udem Th, Holzwarth R, Hänsch T W *Nature* **416** 233 (2002)
26. Serebryannikov E E et al. *Phys. Rev. E* **72** 056603 (2005)
27. Hartl I et al. *Opt. Lett.* **26** 608 (2001)
28. Konorov S O et al. *Phys. Rev. E* **70** 057601 (2004)
29. Ivanov A A, Alfimov M V, Zheltikov A M *Opt. Lett.* **31** 3330 (2006)
30. Sidorov-Biryukov D A, Serebryannikov E E, Zheltikov A M *Opt. Lett.* **31** 2323 (2006)
31. Paulsen H N et al. *Opt. Lett.* **28** 1123 (2003)
32. Kano H, Hamaguchi H *Opt. Express* **13** 1322 (2005)
33. Andresen E R et al. *J. Opt. Soc. Am. B* **22** 1934 (2005)
34. von Vacano B, Wohlleben W, Motzkus M *Opt. Lett.* **31** 413 (2006)
35. Quigley G R, Harris R D, Wilkinson J S *Appl. Opt.* **38** 6036 (1999)
36. Prieto F et al. *J. Lightwave Technol.* **19** 75 (2001)
37. Monro T M et al. *Meas. Sci. Technol.* **12** 854 (2001)
38. Myaing M T et al. *Opt. Lett.* **28** 1224 (2003)
39. Konorov S, Zheltikov A, Scalora M *Opt. Express* **13** 3454 (2005)
40. Rindorf L et al. *Opt. Express* **14** 8224 (2006)
41. Cregan R F et al. *Science* **285** 1537 (1999)
42. Konorov S O et al. *Pis'ma Zh. Eksp. Teor. Fiz.* **76** 401 (2002) [*JETP Lett.* **76** 341 (2002)]
43. Smith C M et al. *Nature* **424** 657 (2003)
44. Zheltikov A M *Usp. Fiz. Nauk* **174** 1301 (2004) [*Phys. Usp.* **47** 1205 (2004)]
45. Konorov S O et al. *Appl. Opt.* **43** 2251 (2004)
46. Konorov S O et al. *J. Phys. D: Appl. Phys.* **36** 1375 (2003)
47. Ouzounov D G et al. *Science* **301** 1702 (2003)
48. Ouzounov D G et al. *Opt. Express* **13** 6153 (2005)
49. Bessonov A D, Zheltikov A M *Phys. Rev. E* **73** 066618 (2006)
50. Serebryannikov E E, Zheltikov A M *Phys. Rev. A* **76** 013820 (2007)
51. Konorov S O et al. *Phys. Rev. E* **70** 066625 (2004)
52. Fedotov A B, Serebryannikov E E, Zheltikov A M *Phys. Rev. A* (in press)
53. Marcatili E A J, Schmeltzer R A *Bell Syst. Tech. J.* **43** 1783 (1964)
54. Zheltikov A M *Usp. Fiz. Nauk* **172** 743 (2002) [*Phys. Usp.* **45** 687 (2002)]
55. Litchinitser N M et al. *Opt. Lett.* **27** 1592 (2002)
56. Litchinitser N M et al. *Opt. Express* **11** 1243 (2003)
57. Roberts P et al. *Opt. Express* **13** 236 (2005)
58. Litchinitser N M, Poliakov E *Appl. Phys. B* **81** 347 (2005)
59. Yariv A, Yeh P *Optical Waves in Crystals* (New York: Wiley, 1984)
60. Nisoli M, De Silvestri S, Svelto O *Appl. Phys. Lett.* **68** 2793 (1996)
61. Nisoli M et al. *Opt. Lett.* **22** 522 (1997)
62. Miyagi M, Nishida S *IEEE Trans. Microwave Theory Tech.* **28** 398 (1980)
63. Miyagi M, Nishida S *IEEE Trans. Microwave Theory Tech.* **28** 536 (1980)
64. Ibanescu M et al. *Science* **289** 415 (2000)
65. Johnson S et al. *Opt. Express* **9** 748 (2001)
66. Konorov S O et al. *Zh. Eksp. Teor. Fiz.* **123** 975 (2003) [*JETP* **96** 857 (2003)]
67. Yeh P, Yariv A, Marom E *J. Opt. Soc. Am.* **68** 1196 (1978)
68. Xu Y, Lee R K, Yariv A *Opt. Lett.* **25** 1756 (2000)
69. Xu Y et al. *J. Lightwave Technol.* **20** 428 (2002)
70. Konorov S O et al. *Phys. Rev. A* **70** 023807 (2004)
71. Konorov S O et al. *Phys. Rev. E* **71** 057603 (2005)
72. Konorov S O et al. *Laser Phys. Lett.* **1** 548 (2004)
73. Fedotov I V, Fedotov A B, Zheltikov A M *Opt. Lett.* **31** 2604 (2006)
74. Benabid F et al. *Science* **298** 399 (2002)
75. Konorov S O, Fedotov A B, Zheltikov A M *Opt. Lett.* **28** 1448 (2003)
76. Benabid F et al. *Nature* **434** 488 (2005)
77. Fedotov A B et al. *Phys. Rev. A* **70** 045802 (2004)
78. Zheltikov A M *Nature Mater.* **4** 267 (2005)
79. Ivanov A A, Podshivalov A A, Zheltikov A M *Opt. Lett.* **31** 3318 (2006)
80. Limpert J et al. *Opt. Express* **11** 3332 (2003)
81. de Matos C J S et al. *Phys. Rev. Lett.* **93** 103901 (2004)
82. Limpert J et al. *IEEE J. Select. Topics Quantum Electron.* **12** 233 (2006)
83. Flusberg B A et al. *Opt. Lett.* **30** 2272 (2005)
84. Zheltikov A M *Appl. Opt.* **47** 474 (2008)
85. Fedotov A B, Beloglazov V I, Zheltikov A M *Ross. Nanotekhnol.* **3** (1 – 2) 61 (2008) [*Nanotechnol. Russ.* **3** 58 (2008)]